Author Manuscript

HHS Public Access

Author manuscript

Magn Reson Med. Author manuscript; available in PMC 2020 January 01.

Published in final edited form as:

Magn Reson Med. 2019 January ; 81(1): 69–78. doi:10.1002/mrm.27514.

Creatine and phosphocreatine mapping of mouse skeletal muscle by a polynomial and Lorentzian line-shape fitting CEST method

Lin Chen[1,2], **Peter B. Barker**[1,2], **Robert G. Weiss**[2,3], **Peter C. M. van Zijl**[1,2], and **Jiadi Xu**[1,2,*]

[1]F.M. Kirby Research Center for Functional Brain Imaging, Kennedy Krieger Research Institute, Baltimore, MD, USA

[2]Russell H. Morgan Department of Radiology and Radiological Science, Johns Hopkins University School of Medicine, Baltimore, MD, USA

[3]Division of Cardiology, Department of Medicine, Johns Hopkins University School of Medicine, Baltimore, MD, USA

Abstract

Purpose: To obtain high-resolution creatine (Cr) and phosphocreatine (PCr) maps of mouse skeletal muscle using a Polynomial and Lorentzian Line-shape Fitting (PLOF) CEST method.

Methods: Wild type (WT) mice and Guanidinoacetate N-Methyltransferase deficient (GAMT−/−) mice that have low Cr and PCr concentrations in muscle were used to assign the Cr and PCr peaks in the Z-spectrum at 11.7 T. A PLOF method was proposed to simultaneously extract and quantify the Cr and PCr by assuming a polynomial function for the background and two Lorentzian functions for the CEST peaks at 1.95 ppm and 2.5 ppm.

Results: The Z-spectra of phantoms revealed that PCr has two CEST peaks (2 ppm and 2.5 ppm), while Cr only showed one peak at 2 ppm. Comparison of the Z-spectra of WT and GAMT−/− mice indicated that, contrary to brain, there was no visible protein guanidinium peak in the skeletal muscle Z-spectrum, which allowed us to extract clean PCr and Cr CEST signals. High-resolution PCr and Cr concentration maps of mouse skeletal muscle were obtained by the PLOF CEST method after calibration with in vivo MRS.

Conclusions: he PLOF method provides an efficient way to map Cr and PCr concentrations simultaneously in the skeletal muscle at high MRI field.

Keywords

Chemical Exchange Saturation Transfer (CEST); Creatine (Cr); Phosphocreatine (PCr); Phosphate Guanidinoacetate (PGua); Guanidinoacetate (Gua); Magnetization Transfer Contrast (MTC); Polynomial and Lorentzian Line-shape Fitting (PLOF); Guanidinoacetate N-Methyltransferase deficiency (GAMT−/−) mouse

[*]**Corresponding Author:** Jiadi Xu, Ph.D., Kennedy Krieger Institute, Johns Hopkins University School of Medicine, 707 N. Broadway, Baltimore, MD, 21205, xuj@kennedykrieger.org, Tel: 443-923-9572, Fax: 443-923-9505.

Author Manuscript Author Manuscript Author Manuscript Author Manuscript

Introduction

Creatine (Cr) and phosphocreatine (PCr) are two primary components of the creatine kinase reaction, arguably the primary energy reserve reaction in muscle (1,2), whereby Cr is phosphorylated to PCr to form a mobilizable reserve of high-energy phosphates (3). Therefore, quantification of the concentrations and tissue distribution of Cr and PCr are important for understanding cellular chemistry and assessing pathologic alterations. The conventional techniques to quantify tissue concentrations of Cr and PCr are ^{1}H and ^{31}P magnetic resonance spectroscopy (MRS). ^{1}H MRS enables the measurement of total Cr (tCr), which is composed of Cr and PCr (4,5). In contrast, ^{31}P MRS is only capable of detecting PCr since Cr does not contain phosphorus (6,7). Despite the success of this technique, MRS quantification is limited by a relatively low signal-to-noise ratio and spatial resolution. In addition, MRS techniques have difficulty in detecting PCr and Cr simultaneously.

The development of the chemical exchange saturation transfer (CEST) method (813) provides an opportunity to detect low concentrations of PCr and Cr in tissues (14,15). One method of Cr CEST uses magnetization transfer ratio asymmetry (MTRasym) analysis, i.e., subtracting the labeling and control images acquired at the two symmetric offsets with respect to water resonance (14–16). This approach is similar to many other CEST applications, such as APT-CEST (17), GlycoCEST (18), GluCEST(19), and gagCEST (20). However, tissue contains many types of exchangeable protons on both sides of the Z-spectrum, such as the amine protons from proteins and glutamate at 2.5 ppm (19,21–23), the hydroxyl groups from proteins and Myo-inositol around 1 ppm (2426), the relayed nuclear Overhauser effect (rNOE) CEST signals from choline at −1.6 ppm (27) and from the aliphatic protons in proteins and lipids between −2 and −4 ppm (20,24,28,29), making asymmetry analysis vulnerable to contaminations from lipids, proteins, semisolid macromolecules and other metabolites.

Another way of estimating the tissue Cr CEST is by acquiring a full Z-spectrum using a continuous wave (CW) RF irradiation with low saturation power and fitting it by assuming a Lorentzian line-shape for the resonances of each exchanging proton pool, including water, amide, guanidinium, and the rNOE peaks (30). This method, however, is still not able to cleanly distinguish the Cr signal from the other CEST signals, such as the amine and aromatic protons at 2 ppm (31). In addition to the CW-CEST, a pulsed-CEST method dubbed chemical exchange rotation transfer (CERT) (32,33) has been developed to selectively detect slow to intermediate exchanging protons. CERT has the potential to selectively map Cr and PCr signals with minor contaminations from proteins (34), which also contain some guanidinium protons resonating at 2 ppm. Recently, a Cr CEST study carried out on guanidinoacetate methyltransferase deficient (GAMT−/−) mouse brain showed that the tCr signal contributes only part of the guanidinium peak at 1.95 ppm (35), a finding consistent with an ex vivo study using homogenous rat brain tissue (36). Based on these findings, we developed a polynomial and Lorentzian line-shape fitting (PLOF) method to extract and quantify the tCr signal in the brain (35). This new method is assumed to remove most contaminations to the tCr CEST signal except for a small portion of signal from the protein guanidinium protons.

Author Manuscript Author Manuscript Author Manuscript Author Manuscript

In the current study, we extend the PLOF method to map the PCr and Cr concentrations simultaneously in mouse skeletal muscle. Although the CEST signals at 2 ppm and 2.5 ppm have been shown to be related to Cr and PCr, the accurate quantification of Cr and PCr still faces several challenges. Firstly, the concentrations of PCr, Cr and mobile proteins in skeletal muscle are quite different from those in the brain. In previous studies, the lack of an efficient way to extract the PCr and Cr signals from the skeletal muscle Z-spectrum was primarily due to the uncertainty of the amount of the Cr and PCr contributions in the Z-spectrum. In this study, we used GAMT–/– mice to verify the contribution of the Cr and PCr signal to the muscle CEST Z-spectrum. Secondly, the acquisition parameters to maximize CEST contrast of Cr and PCr in skeletal muscle are significantly different from those for phantom studies due to the abundance of semisolid macromolecular tissue components. In this study, we optimized the saturation power to obtain the maximum CEST contrast of Cr and PCr in skeletal muscle at 11.7 T. Thirdly, the PLOF method is a recently proposed CEST quantification method that has been validated for obtaining high-resolution Cr maps in mouse brain. However, the initial PLOF method used for brain is not suitable for the two-peak case in this muscle study, where CEST signal at 2.5 ppm contains the contribution from PCr, while CEST signal at 2 ppm contains the contributions from both Cr and PCr. Here we propose an improved PLOF method to resolve this problem and yield both high-resolution Cr and PCr concentration maps.

Methods

MRI Experiments

All MRI experiments were performed on a horizontal bore 11.7 T Bruker Biospec system (Bruker, Ettlingen, Germany). For the animal studies, a 72 mm quadrature volume resonator was used as a transmitter and a four-element (2×2) phased array coil was used as a receiver. A 23 mm volume transceiver coil was used for the phantom studies. Six saturation powers (0.3 μT, 0.6 μT, 0.8 μT, 1 μT, 1.5 μT and 2 μT) were used for the optimization of the PCr/Cr CEST signals. According to previous studies, the steady-state condition, at which the CEST signal will not increase with longer saturation length, was determined by the values at each saturation power (35,39,40). Saturation lengths of 4 s for 0.3 – 0.8 μT power, 3 s for 1 – 1.5 μT power, and 2 s for 2 μT power will reach the steady-state saturation and were applied in the current study. The saturation offsets were swept from −7 to 5 ppm with an increment of 0.2 ppm. Here, −7 ppm was chosen due to the broad peaks from semisolid components with a center frequency in the aliphatic range. A 0.05 ppm increment was used between 1.5 ppm and 2.8 ppm to facilitate the fitting of the PCr/Cr CEST signals. MR images were acquired using a Turbo Spin Echo (TSE) sequence with TE = 3.7 ms, TSE factor = 16, slice thickness =1.5 mm, a matrix size of 64×32 and a resolution of 0.25×0.25 mm^2. The B_0 field over the mouse brain was adjusted using field-mapping and second-order shimming. The R_1 relaxation of the mouse brain was measured using variable TR RARE (RAREVTR) (TR = 5.5, 3.0, 1.5, 0.8, 0.5, 0.3 s). The in vivo MRS experiments were performed on a voxel of 2 × 2 × 2 mm^3 using a stimulated echo acquisition mode (STEAM) sequence (TE = 3 ms, TM = 10 ms, TR = 2.5 s, NA = 256) following the experimental parameters given previously (35).

Author Manuscript Author Manuscript Author Manuscript Author Manuscript

Freshly made phantoms with Cr (5, 10, 20 and 30 mM), PCr (5, 10, 20 and 30 mM), and guanidinoacetate (Gua) (30 mM) solutions were used to investigate the power and concentration dependence of the CEST contributions of guanidinium proton containing compounds in muscle. Notice that phosphorylated guanidinoacetate (PGua) protons contribute to the CEST Z-spectrum of the GAMT−/− mouse. However, PGua is not commercially available. The above three components (Cr, PCr and Gua) were used to assign the in vivo CEST peaks. All phantoms were prepared in phosphate buffered saline (PBS), titrated to pH 7.0. The phantoms were maintained at 37°C during the MRI experiments with an air heater. A calibration phantom with 20 mM Cr mixed with crosslinked bovine serum albumin (BSA) (20% w, pH=7.2) was used for the MRS quantification. The BSA was crosslinked using glutaraldehyde following a previously described procedure (41). The T_1 relaxation time of water protons in the cross-linked BSA (T_1 = 1.8 s) is close to that of mouse muscle (T_1 = 1.9 s) at 11.7 T. Although the T_2 value (T_2 = 46 ms) in the cross-linked BSA is higher than that in muscle (T_2=26 ms), the impact on the MRS quantification is minimized due to the short TE STEAM method applied.

Animal Studies

The institutional animal care and use committee approved this study. Three adult female BALB/c mice (14 months) as wild type (WT) mice and three GAMT−/− mice (14 months) were used. The tCr of GAMT−/− mouse muscle is significantly reduced compared to the WT counterpart (42–46). However, the amount of PGua is still considerable, as confirmed by a ^{31}P MRS study (42). All animals were induced using 2% vaporized inhaled isoflurane, followed by 1.5% isoflurane during the MRI scan.

Cr and PCr Quantification Using the Two-peak PLOF method

For the *in vivo* CEST studies, the observed CEST peak is scaled down by a factor of Z^2 compared to the signal from the phantom (35), where Z is the normalized value of the steady-state Z-spectrum. This scale-down effect, dubbed the spillover effect, is determined by the tissue macromolecule concentrations and the applied saturation parameters (40,47–50). The PLOF quantification method based on the $R_{1\rho}$ relaxation theory is robust against the spillover effect (35). In the current study, a two-peak PLOF method is designed to extract and quantify the PCr and Cr CEST signals simultaneously. In the framework of the $R_{1\rho}$ relaxation theory, the normalized saturation signal Z^{ss} (i.e., the water saturation signal S normalized by the signal without saturation, S_0) at steadystate for each offset is given by (39,40,47):

$$Z^{ss} = \frac{cos^2\theta R_1}{R_{1\rho}} \quad (1)$$

where R_1 is the longitudinal relaxation rate of water and $\theta = tan^{-1}\ \omega_1/$ is the tilt angle of the effective magnetization with respect to the z-axis induced by the radio frequency (RF) saturation with a nutation frequency of ω_1 and an offset of . $R_{1\rho}$ is the water relaxation rate under RF saturation, which contains the contributions from the effective water relaxation

Author Manuscript Author Manuscript Author Manuscript Author Manuscript

accounting for the direct saturation effect in the Z-spectra and an apparent relaxation term due to all the saturation transfer processes in the tissue (40).

$$R_{1\rho} = R_{eff} + R_{back} + R_{peak1} + R_{peak2} \quad (2)$$

where $R_{eff} = cos^2\theta R_1 + sin^2\theta R_2$ is the longitudinal relaxation rate of water in the rotating frame without additional solutes. R_{back} is the background pool that includes the water direct saturation (DS), the magnetization transfer contrast (MTC), the aromatic protons and the other metabolites. R_{peak1} and R_{peak2} are the introduced rotational frame relaxation rates of the two targeted CEST peaks. In the current study, these are the peaks at 1.95 ppm (Cr+PCr) and 2.5 ppm (PCr), respectively. The Z-spectrum can be fitted using Eqs.1&2 by assuming R_{peak1} and R_{peak2} as two Lorentzian functions and the R_{back} as a third-order polynomial function (51):

$$R_{peak1} = R_{peak1}^{max} \frac{(w_{peak1}/2)^2}{(w_{peak1}/2)^2 + (\Delta - \Delta_{peak1})^2} \quad (3)$$

$$R_{peak2} = R_{peak2}^{max} \frac{(w_{peak2}/2)^2}{(w_{peak2}/2)^2 + (\Delta - \Delta_{peak2})^2} \quad (4)$$

$$R_{back} = D0 + D1(\Delta - 2) + D2(\Delta - 2)^2 + D3(\Delta - 2)^3 \quad (5)$$

where w_{peak1} and w_{peak2} are the peak full-width-at-half-maximum of the Lorentzian line-shape. R_{peak1}^{max} and R_{peak2}^{max} refer to the true apparent relaxation rate. Chemical shift offsets are represented by $_{peak1}$ and $_{peak2}$. The terms $D0$ to $D3$ are the zero to thirdorder polynomial coefficients.

A two-step fitting strategy was applied to fit the Z-spectrum. The first step fits the background of the steady-state Z-spectrum Z_{back}^{ss} without the two CEST peaks, i.e., $R_{peak1} = R_{peak2} = 0$. Under the steady-state situation, the Z-spectrum Z_{back}^{ss} is R_{back} correlated to with Eq.1 and is given by:

$$Z_{back}^{ss} = \frac{cos^2\theta R_1}{R_{eff} + R_{back}} \quad (6)$$

Combining Eqs. 5 and 6, the Z_{back}^{ss} can be fitted by varying the polynomial coefficients $D0$ – $D3$. The second step fits the targeted peaks with the fixed background Z_{back}^{ss}, i.e., R_{back}. The fitting of Z^{ss} was accomplished by varying the parameters w_{peak1}/w_{peak2}, $_{peak1}/$ $_{peak2}$, and $R_{peak1}^{max}/R_{peak2}^{max}$ according to

$$Z^{ss} = \frac{cos^2\theta R_1}{R_{eff} + R_{back} + R_{peak1} + R_{peak2}} \quad (7)$$

For the PCr and Cr mapping, the initial chemical shift offsets were set to 1.95 ppm and 2.5 ppm. The Z-spectrum between 1.3 and 3.4 ppm was utilized for the two-step fitting, and three regions of the Z-spectrum, i.e., 1.3–1.7 ppm, 2.25–2.35 ppm and 2.83–3.4 ppm, were selected for the background fitting. PCr is the main contributor to the CEST peak at 2.5 ppm, while the peak at 1.95 ppm contains both Cr and PCr. Therefore, the PCr signal rate (R_{PCr}^{max}) is given by the CEST peak at 2.5 ppm ($R_{2.5}^{max}$), i.e., $R_{PCr}^{max} = R_{2.5}^{max}$, while the Cr signal ($R_{Cr}^{max}$) needs to be obtained by subtracting the PCr contribution from the 1.95 ppm CEST signal ($R_{1.95}^{max}$) using

$$R_{Cr}^{max} = R_{1.95}^{max} - F_{PCr} \cdot R_{2.5}^{max} \quad (8)$$

where F_{pcr} refers to the CEST signal ratio between the two peaks of the PCr CEST signal ($F_{PCr} = R_{pCr,\,1.95}^{max}/R_{pCr,\,2.5}^{max}$) and can be obtained from the Z-spectrum of the PCr phantom. The R_{Cr}^{max} and R_{PCr}^{max} can be correlated to the Cr and PCr concentrations $[Cr]$ and $[PCr]$ obtained from MRS through the following relationship:

$$R_{cr}^{max} = r_{Cr} \cdot [Cr] \quad (9)$$

$$R_{Pcr}^{max} = r_{PCr} \cdot [PCr] \quad (10)$$

where r_{cr} and r_{PCr} are the apparent relaxivities (expressed in $s^{-1}mM^{-1}$) of Cr and PCr, respectively, which are analogous to the relaxivity terms used for contrast agent studies. The normalized mean square error (NMSE) was utilized to objectively evaluate the goodness of the PLOF fit between estimated and measured data, of which the definition is given below:

$$NMSE = 1 - \frac{\left\| S_{ref} - S_{fit} \right\|^2}{\left\| S_{ref} - mean(S_{ref}) \right\|^2} \quad (11)$$

Author Manuscript Author Manuscript Author Manuscript Author Manuscript

where ‖ ‖ indicates the 2-norm of a vector, S_{ref} refers to the observed CEST signals and S_{fit} stands for the fitting result obtained by PLOF method. NMSE varies between minus infinity (bad fit) to 1 (perfect fit).

The Cr and PCr concentrations from the in vivo ^{1}H MRS spectra were estimated using the LCModel method (52,53). The tCr concentration was obtained from the ratio (g) between the area under a best fit tCr spectrum in the LCModel on muscle and on the calibration phantom (20 mM Cr in cross-linked BSA) as g 20 mM . Possible contributions of the Cr signals that are invisible in MRS due to binding effects with the cross-linked BSA were neglected in the current study. Taurine (Tau) is a high concentration metabolite in muscle that shows strong and broad CEST signal around 2 ppm. Hence, the concentrations of Tau in both WT and GAMT−/− mice were also determined by MRS using the ratio between Tau and the tCr in the calibration phantom as obtained by the LCModel. Due to the overlap of the Cr and PCr signals in the proton spectrum, the concentration ratio between them is hard to determine by high-resolution in vivo ^{1}H MRS. In the literature, an approximate ratio of 1: 3 has been reported for the Cr/PCr ratio in skeletal muscle (Cr 7.5 mM: PCr 22.5 mM) (54,55). This ratio was used for quantifying the Cr and PCr concentrations in this study.

The observed CEST signals at 2.5 ppm ($Z_{2.5}$) and 1.95 ppm ($Z_{1.95}$) were calculated by $\Delta Z_{2.5} = Z^{ss}_{back} - Z^{ss}_{2.5}$, $\Delta Z_{1.95} = Z^{ss}_{back} - Z^{ss}_{1.95}$. The observed amide proton peak ($Z_{3.6}$) was estimated by fitting the Z values at 3.1–3.2 ppm and 4.2–4.8 ppm using a first order linear function. Then, the $Z_{3.6}$ was calculated by taking the difference between the fitted background (Z^{ss}_{back}) and the observed Z value at the 3.6 ppm, i.e., ($Z^{ss}_{back} - Z^{ss}_{3.6}$).

Results

MRS of the Skeletal Muscle

Typical in vivo ^{1}H MRS of the skeletal muscle of WT and GAMT−/− mice are shown in Fig. 1. High-resolution T_2 weighted images by the RARE sequence are included for anatomical guidance. From the spectra it can be seen that the tCr signals of the GAMT−/− skeletal muscle at 3 ppm and 3.9 ppm are significantly reduced compared to those of the WT mouse ($p<0.001$). The tCr concentrations estimated by the LCModel method were 38.8±2.8 mM and 1.2±0.8 mM for the WT and GAMT−/− mice (n=3), respectively. A weak and broad peak from PGua can be seen at 3.78 ppm (42). The Tau concentrations were identical for the WT (58.3 ± 1.6 mM) and the GAMT−/− (58.3 ± 1.6 mM) mice.

Z-spectra of the Phantoms and the Skeletal Muscle

The Z-spectra of the 30 mM Cr, PCr, and Gua phantoms at pH = 7.0 recorded with 1 μT saturation power are shown in Fig. 2A. There is one strong peak around 2.0 ppm present in the Cr CEST Z-spectrum, while two peaks around 2.0 ppm and 2.5 ppm are observed in the PCr CEST Z-spectrum. The PCr CEST signal around 2.5 ppm is about 3.0 ± 0.2 % of the water magnetization, which is much stronger than the signal at 2 ppm (about 1.8 ± 0.2 % of water magnetization). Using MTR_{asym} analysis, the contribution ratio F_{PCr} between the two peaks of the PCr CEST was determined to be 0.55± 0.02 (1.8± 0.2% : 3.0± 0.1%). The Cr CEST signal around 2 ppm (about 11.7 ± 0.5 % of water proton magnetization) is far

Author Manuscript Author Manuscript Author Manuscript Author Manuscript

stronger than its PCr counterpart. For the CEST Z-spectrum of Gua, a strong CEST signal (12.5 ± 0.5%) can be also found at 2 ppm. The concentration dependencies of R_{cr}^{max} (2.5 ppm) and R_{Pcr}^{max} (2.5 ppm) were also determined from the Cr and PCr CEST effects in phantoms using Eq.1 and the determined R_1. For these concentration studies in vitro (Fig. 2B), both Cr and PCr R_{cr}^{max} are linearly dependent on the concentration up to about 30 mM.

Fig. 2C shows the comparison between the Z-spectra of the GAMT –/– and WT mice with a saturation power of 1 μT. To eliminate the mismatch of the Z-spectra due to the B_1 variation across the experiments, the Z-spectra were aligned on the intensity scale using the Z-spectral intensity at 5 ppm (35). The MTC background change induced by B_1 inhomogeneity is about 2% of the water signal, which is comparable to the CEST contrasts of Cr and PCr. Hence, the intensity alignment was carried out to give a better comparison. The saturation offset was aligned using the signals around 0 ppm. Notable differences were observed for the Z-spectra of the GAMT –/– and WT mice between 1 – 3 ppm. The Z-spectrum of the WT mice showed two clear peaks around 1.95 ppm and 2.5 ppm, while there was only one sharp peak around 2.2 ppm in the Z-spectrum of the GAMT–/– mice. This confirms the observation by previous MRS studies on GAMT–/– mice that the concentration of Gua is negligible in the WT mouse muscle while a high concentration of PGua is present in GAMT –/– (42). The full Z-spectra of the GAMT–/– and WT mice with different saturation powers are shown in Figs. 2D&E, respectively. It can be seen from these that there are strong aliphatic peaks at the right side from 0 to −5 ppm with an approximate maximum peak around −3.6 ppm. The complicated line-shape of this composite aliphatic peak may degrade the accuracy of the PCr and Cr quantification if one were to use the asymmetry analysis method, such as indicated in Fig. 2F.

CEST Signal Extraction and Optimization

The fitting using the PLOF method is demonstrated in Figs. 3A&B. The PLOF method fits the background and extracts the $R_{2.5}$ and $R_{1.95}$ curves. To determine the optimal saturation power for the *in vivo* Cr and PCr CW-CEST experiments, the CEST signals at 3.6 ppm ($Z_{3.6}$), 2.5 ppm ($Z_{2.5}$), and 1.95 ppm ($Z_{1.95}$) were measured as a function of saturation power (Fig. 3C). The strongest $Z_{3.6}$ was observed at 0.6 μT with a maximum value around 1.2 ± 0.3 % that dropped quickly with higher saturation power. At 1 μT, the $Z_{3.6}$ decreased to 0.8 ± 0.16 % for muscle, which is much smaller than the $Z_{3.6}$ of mouse brain (1.55 ± 0.05 %) at the same saturation power (35). The maximum $Z_{2.5}$ and $Z_{1.95}$ were observed at about 1 μT. Similar to the tCr CEST study on mouse brain (35), the observed CEST signals at 2.5 and 1.95 ppm quickly decreased with the increase in saturation power due to the spill-over from MTC and the other CEST signals. According to the theory of $R_{1\rho}$, the extracted $R_{1.95}^{max}$ and $R_{2.5}^{max}$ are immune to the spillover effect. As indicated in Fig. 3D, the extracted $R_{1.95}^{max}$ values showed an increase with respect to saturation power, while the PCr signal $R_{2.5}^{max}$ increased first and then plateaued after 1 μT due to its much smaller exchange rate (i.e. fully labeled with saturation powers higher than 1 μT).

Author Manuscript Author Manuscript Author Manuscript Author Manuscript

PCr and Cr Concentration Maps

The extracted $R_{1.95}^{max}$ and $R_{2.5}^{max}$ maps of skeletal muscle at a saturation power of 1 μT are shown in Figs. 4B&C, respectively. The r_{Cr} and r_{PCr} were determined to be 2.85 ± 0.05 · 10^{-3} $s^{-1}mM^{-1}$ and 0.75 ± 0.05 · $s^{-1}mM^{-1}$ at a saturation power of 1 μT, respectively. The concentration maps of Cr and PCr obtained using Eqs. 8&9 are shown in Figs. 4D&E, respectively. The goodness of the PLOF fitting for each pixel is illustrated by the NMSE map shown in Fig. 4F. The mean value and standard deviation of the NMSE map are 0.9922 and 0.0034, respectively. The averaged Cr and PCr concentrations of the mouse calf muscle were determined to be 11.3 ± 1.4 mM and 30.8 ± 2.8 mM, respectively, which are slightly higher than previously reported values (Cr 7.5 mM : PCr 22.5 mM) from spectroscopy (54,55). Due to the relatively low resolution of the PCr and Cr maps, the maps are not following any pattern of muscle anatomy. Also, the edges of the PCr and Cr maps (transition from muscle to air) show strong concentration gradients due to the partial volume effect.

Discussion

The current study demonstrates the use of a two-peak PLOF method to yield PCr and Cr concentration maps. The Z-spectra in Fig. 2 and the analysis of the results in Fig. 3 indicate that a mobile protein guanidium peak is undetectable and the amide peak is small with a maximum amplitude of around 1.2% of water magnetization in skeletal muscle. This is quite different from the previous brain studies, where amide and guanidinium peaks are commonly observed due to the abundance of mobile proteins in brain tissue. The disappearance of the protein guanidinium peak and the reduction of the amide peaks from the proteins are favorable to the extraction of clean Cr and PCr CEST signal. The skeletal muscle Z-spectrum between 0 to −3.6 ppm was still dominated by the relayed nuclear Overhauser enhancement (rNOE) signal arising from the aliphatic protons of glycogen, proteins and lipids.

The extraction of Cr and PCr CEST signal provides an opportunity to optimize the acquisition scheme for in vivo Cr and PCr CEST applications at 11.7T. This study together with the previous mouse brain study (35) demonstrates that the observed CEST signals of PCr and Cr in tissues are different from those in phantoms. After reaching a maximum value at 1 μT, the observed muscle PCr and Cr CEST signals quickly decreased with an increase in saturation power, as shown in Fig. 3. However, for the phantom studies, the PCr and Cr CEST signals increased when the saturation power rose above 1 μT (38). This phenomenon can be explained by the spillover effect induced by the background signals from direct saturation (DS) and semi-solid magnetization transfer contrast (MTC) effects as indicated in the previous study (35):

$$\Delta Z_{obs} = {Z_{back}^{ss}}^2 (1 - Z_{clean}) \quad (12)$$

where (1 - Z_{clean}) is the clean CEST signal without MTC and DS, and Z_{obs} is the observed PCr or Cr CEST signal. For the Cr/PCr CEST signals, the saturation efficiency is proportional to the saturation power initially, and then levels off slowly until reaching

Author Manuscript

maximum saturation (see Fig. 3D). However, the MTC increases stronger with saturation powers, leading to an increase in Z_{back}^{ss}. As a result, the observed CEST signal will drop quickly at higher saturation powers, as predicted in Eq. 12. A similar power dependence of CEST signal has also been observed for other slow-exchanging protons, such as rNOE CEST (41).

The signal-to-noise ratio of the PCr and Cr CEST (SNR_{CEST}) can be estimated by the CEST signal ($Z_{Cr/Pcr}$) and the standard deviation of the residual fitting signal from the PLOF method (Std_{PLOF}) using $SNR_{CEST=}$ $Z_{Cr/Pcr}/Std_{PLOF}$. The residual fitting signal was extracted from the region between 2.9 ppm and 3.5 ppm by subtracting the fitted Z^{ss} and the experimental Z-spectrum. The SNR_{CEST} values were found to be 38.5 and 19.5 for Cr and PCr for a voxel volume of 8 mm^3 (slice thickness 1.5 mm and ROI area 5.3 mm^2), respectively. As a comparison, the SNR values for the Cr and PCr peak measured by MRS with same voxel volume (2×2×2 mm^3) and a same experimental time as CEST experiments (5 minutes) were 2.6 ± 0.5 and 8 ± 0.5, respectively. Therefore, the SNR gain using CEST is about 14.8 times higher than the MRS method for Cr, while PCr is about 2.4 times higher. The CEST SNR can be further improved by either applying a more stable image acquisition module or optimizing the CEST labeling scheme.

The proposed PLOF method is ready to be transferred directly to 7T MRI scanners. However, we expect some challenges when applying PLOF to simultaneously obtain PCr and Cr maps on 3T scanners. Due to the fast exchange rate of guanidinium protons in Cr, the CEST signal at 2 ppm is broad and starting to coalesce with the water peak. The detection of PCr at 3T systems is possible due to its relatively slow guanidinium proton exchange rate (120±50 Hz) and larger offset difference with water. The saturation power therefore needs to be reduced at 3T and, in consideration of the water direct saturation, a saturation power between 0.5 μT and 0.7 μT and a duration between 800 ms and 1 s is estimated to be suitable for PCr CEST experiments on a 3T scanner. We attribute the lack of a PCr signal in previous CEST studies (15) at 3T to the strong saturation power applied. With strong saturation power, the CEST peaks of PCr and Cr merge with each other and the background MTC, DS and glycogen signals and appear to be one broad CEST signal. Due to the faster exchange rate of guanidinium proton in Cr, the CEST contrast of Cr is much stronger compared to that of PCr at the same concentration. Therefore, though both PCr and Cr contribute to MTR_{asym} signal at 2 ppm, the signal change during leg exercise is dominated by the Cr.

Conclusions

In this study, skeletal muscle PCr and Cr CEST signal concentrations were determined by comparing Z-spectra recorded on WT and GAMT−/− mice. The CEST peak at 1.95 ppm contains contributions from both Cr and PCr, while the CEST peak at 2.5 ppm is primarily the result of PCr. The CEST signal originating from protein guanidinium protons is not detectable in skeletal muscle, which is favorable for the extraction of clean PCr and Cr CEST signals. PCr and Cr maps of skeletal muscle could be obtained simultaneously using the proposed PLOF method

Author Manuscript Author Manuscript Author Manuscript Author Manuscript

Acknowledgments

This work was supported by R01EB015032, P41EB015909, and R01HL63030. The authors thank Dirk Isenbrandt for creating and providing the GAMT−/− mice.

Grant support from NIH: R01EB015032, P41EB015909, and R01HL63030

References:

1. Wyss M, Kaddurah-daouk R. Creatine and Creatinine Metabolism. Physiol Rev 2000;80:1107. [PubMed: 10893433]
2. Andres RH, Ducray AD, Schlattner U, Wallimann T, Widmer HR. Functions and effects of creatine in the central nervous system. Brain Res Bull 2008;76(4):329–343. [PubMed: 18502307]
3. Schlattner U, Tokarska-Schlattner M, Wallimann T. Mitochondrial creatine kinase in human health and disease. Biochim Biophys Acta 2006;1762(2):164–180. [PubMed: 16236486]
4. Boesch C Musculoskeletal spectroscopy. J Magn Reson Imaging 2007;25(2):321–338. [PubMed: 17260389]
5. Bottomley PA, Lee Y, Weiss RG. Total creatine in muscle: imaging and quantification with proton MR spectroscopy. Radiology 1997;204(2):403–410. [PubMed: 9240527]
6. Prompers JJ, Jeneson JA, Drost MR, Oomens CC, Strijkers GJ, Nicolay K. Dynamic MRS and MRI of skeletal muscle function and biomechanics. NMR Biomed 2006;19(7):927–953. [PubMed: 17075956]
7. Kemp GJ, Meyerspeer M, Moser E. Absolute quantification of phosphorus metabolite concentrations in human muscle in vivo by 31P MRS: a quantitative review. NMR Biomed 2007;20(6):555–565. [PubMed: 17628042]
8. Wolff S, Balaban R. NMR imaging of labile proton exchange. J Magn Reson 1990;86:164–169.
9. van Zijl PCM, Yadav NN. Chemical exchange saturation transfer (CEST): What is in a name and what isn’t? Magn Reson Med 2011;65(4):927–948. [PubMed: 21337419]
10. van Zijl PCM, Lam WW, Xu J, Knutsson L, Stanisz GJ. Magnetization Transfer Contrast and Chemical Exchange Saturation Transfer MRI. Features and analysis of the field-dependent saturation spectrum. Neuroimage 2017:10.1016/j.neuroimage.2017.1004.1045.
11. Liu G, Song X, Chan KW, McMahon MT. Nuts and bolts of chemical exchange saturation transfer MRI. NMR Biomed 2013;26(7):810–828. [PubMed: 23303716]
12. Jones KM, Pollard AC, Pagel MD. Clinical applications of chemical exchange saturation transfer (CEST) MRI. J Magn Reson Imaging 2017:10.1002/jmri.25838.
13. van Zijl PCM, Sehgal AA. Proton Chemical Exchange Saturation Transfer (CEST) MRS and MRI. eMagRes 2016;5(2):1–26.
14. Haris M, Nanga RP, Singh A, Cai K, Kogan F, Hariharan H, Reddy R. Exchange rates of creatine kinase metabolites: feasibility of imaging creatine by chemical exchange saturation transfer MRI. NMR Biomed 2012;25(11):1305–1309. [PubMed: 22431193]
15. Haris M, Singh A, Cai K, Kogan F, McGarvey J, Debrosse C, Zsido GA, Witschey WR, Koomalsingh K, Pilla JJ, Chirinos JA, Ferrari VA, Gorman JH, Hariharan H, Gorman RC, Reddy R. A technique for in vivo mapping of myocardial creatine kinase metabolism. Nat Med 2014;20(2):209–214. [PubMed: 24412924]
16. Zu Z, Louie EA, Lin EC, Jiang X, Does MD, Gore JC, Gochberg DF. Chemical exchange rotation transfer imaging of intermediate-exchanging amines at 2 ppm. NMR Biomed 2017;30(10): 10.1002/nbm.3756.
17. Zhou J, Payen JF, Wilson DA, Traystman RJ, van Zijl PC. Using the amide proton signals of intracellular proteins and peptides to detect pH effects in MRI. Nat Med 2003;9(8):1085–1090. [PubMed: 12872167]
18. van Zijl PC, Jones CK, Ren J, Malloy CR, Sherry AD. MRI detection of glycogen in vivo by using chemical exchange saturation transfer imaging (glycoCEST). Proc Natl Acad Sci U S A 2007;104(11):4359–4364. [PubMed: 17360529]

Author Manuscript Author Manuscript Author Manuscript Author Manuscript

19. Cai K, Haris M, Singh A, Kogan F, Greenberg JH, Hariharan H, Detre JA, Reddy R. Magnetic resonance imaging of glutamate. Nat Med 2012;18(2):302–306. [PubMed: 22270722]
20. Ling W, Regatte RR, Navon G, Jerschow A. Assessment of glycosaminoglycan concentration in vivo by chemical exchange-dependent saturation transfer (gagCEST). Proc Natl Acad Sci U S A 2008;105(7):2266–2270. [PubMed: 18268341]
21. Jin T, Wang P, Zong X, Kim S-G. Magnetic resonance imaging of the Amine–Proton Exchange (APEX) dependent contrast. NeuroImage 2012;59(2):1218–1227. [PubMed: 21871570]
22. Zong X, Wang P, Kim SG, Jin T. Sensitivity and source of amine-proton exchange and amideproton transfer magnetic resonance imaging in cerebral ischemia. Magn Reson Med 2014;71(1):118–132. [PubMed: 23401310]
23. Davis KA, Nanga RP, Das S, Chen SH, Hadar PN, Pollard JR, Lucas TH, Shinohara RT, Litt B, Hariharan H, Elliott MA, Detre JA, Reddy R. Glutamate imaging (GluCEST) lateralizes epileptic foci in nonlesional temporal lobe epilepsy. Sci Transl Med 2015;7(309):309ra161.
24. Chen L, Xu X, Zeng H, Chan K, Yadav NN, Cai S, Schunke KJ, Faraday N, van Zijl PCM, Xu J. Separating Fast and Slow Exchange Transfer and Magnetization Transfer Using Offresonance Variable Delay Multiple Pulse (VDMP) MRI. Magn Reson Med 2018:101002/mrm.27111.
25. Zaiss M, Windschuh J, Goerke S, Paech D, Meissner JE, Burth S, Kickingereder P, Wick W, Bendszus M, Schlemmer HP, Ladd ME, Bachert P, Radbruch A. Downfield-NOE-suppressed amide-CEST-MRI at 7 Tesla provides a unique contrast in human glioblastoma. Magn Reson Med 2017;77(1):196–208. [PubMed: 26845067]
26. Haris M, Singh A, Cai K, Nath K, Crescenzi R, Kogan F, Hariharan H, Reddy R. MICEST: a potential tool for non-invasive detection of molecular changes in Alzheimer's disease. J Neurosci Methods 2013;212(1):87–93. [PubMed: 23041110]
27. Zhang XY, Wang F, Afzal A, Xu J, Gore JC, Gochberg DF, Zu Z. A new NOE-mediated MT signal at around −1.6ppm for detecting ischemic stroke in rat brain. Magn Reson Imaging 2016;34(8): 1100–1106. [PubMed: 27211260]
28. Jones CK, Huang A, Xu J, Edden RA, Schar M, Hua J, Oskolkov N, Zaca D, Zhou J, McMahon MT, Pillai JJ, van Zijl PC. Nuclear Overhauser enhancement (NOE) imaging in the human brain at 7T. NeuroImage 2013;77C:114–124.
29. Xu J, Yadav NN, Bar-Shir A, Jones CK, Chan KW, Zhang J, Walczak P, McMahon MT, van Zijl PC. Variable delay multi-pulse train for fast chemical exchange saturation transfer and relayednuclear overhauser enhancement MRI. Magn Reson Med 2014;71(5):1798–1812. [PubMed: 23813483]
30. Cai K, Singh A, Poptani H, Li W, Yang S, Lu Y, Hariharan H, Zhou XJ, Reddy R. CEST signal at 2ppm (CEST@2ppm) from Z-spectral fitting correlates with creatine distribution in brain tumor. NMR Biomed 2015;28(1):1–8. [PubMed: 25295758]
31. Desmond KL, Moosvi F, Stanisz GJ. Mapping of amide, amine, and aliphatic peaks in the CEST spectra of murine xenografts at 7 T. Magn Reson Med 2014;71(5):1841–1853. [PubMed: 23801344]
32. Zu Z, Janve VA, Xu J, Does MD, Gore JC, Gochberg DF. A new method for detecting exchanging amide protons using chemical exchange rotation transfer. Magn Reson Med 2013;69(3):637–647. [PubMed: 22505325]
33. Zu Z, Janve VA, Li K, Does MD, Gore JC, Gochberg DF. Multi-angle ratiometric approach to measure chemical exchange in amide proton transfer imaging. Magn Reson Med 2012;68(3):711–719. [PubMed: 22161770]
34. Zu Z, Lin E, Louie E, Jiang X, Lankford C, Damon B, Does M, Gore J, Gochberg D. Chemical Exchange Rotation Transfer imaging of Phosphocreatine in Muscle. 2018; Paris, France Proceedings of the 26h Annual Meeting of ISMRM p 5106.
35. Chen L, Zeng H, Xu X, Yadav NN, Cai S, Puts NA, Barker PB, Li T, Weiss RG, van Zijl PCM, Xu J. Investigation of the contribution of total creatine to the CEST Z-spectrum of brain using a knockout mouse model. NMR Biomed 2017;30(12):101002/nbm.3834.
36. Zhang XY, Xie J, Wang F, Lin EC, Xu J, Gochberg DF, Gore JC, Zu Z. Assignment of the molecular origins of CEST signals at 2 ppm in rat brain. Magn Reson Med 2017;78(3):881–887. [PubMed: 28653349]

Author Manuscript Author Manuscript Author Manuscript Author Manuscript

37. Kogan F, Haris M, Debrosse C, Singh A, Nanga RP, Cai K, Hariharan H, Reddy R. In vivo chemical exchange saturation transfer imaging of creatine (CrCEST) in skeletal muscle at 3T. J Magn Reson Imaging 2014;40(3):596–602. [PubMed: 24925857]
38. Rerich E, Zaiss M, Korzowski A, Ladd ME, Bachert P. Relaxation-compensated CEST-MRI at 7 T for mapping of creatine content and pH--preliminary application in human muscle tissue in vivo. NMR Biomed 2015;28(11):1402–1412. [PubMed: 26374674]
39. Jin T, Autio J, Obata T, Kim S-G. Spin-locking versus chemical exchange saturation transfer MRI for investigating chemical exchange process between water and labile metabolite protons. Magn Reson Med 2011;65(5):1448–1460. [PubMed: 21500270]
40. Zaiss M, Bachert P. Chemical exchange saturation transfer (CEST) and MR Z-spectroscopy in vivo: a review of theoretical approaches and methods. Phys Med Biol 2013;58(22):R221–269. [PubMed: 24201125]
41. Yadav NN, Yang X, Li Y, Li W, Liu G, van Zijl PCM. Detection of dynamic substrate binding using MRI. Scientific Reports 2017;7(1):10138. [PubMed: 28860625]
42. Renema WK, Schmidt A, van Asten JJ, Oerlemans F, Ullrich K, Wieringa B, Isbrandt D, Heerschap A. MR spectroscopy of muscle and brain in guanidinoacetate methyltransferase (GAMT)-deficient mice: validation of an animal model to study creatine deficiency. Magn Reson Med 2003;50(5):936–943. [PubMed: 14587004]
43. Skelton MR, Schaefer TL, Graham DL, Degrauw TJ, Clark JF, Williams MT, Vorhees CV. Creatine transporter (CrT; Slc6a8) knockout mice as a model of human CrT deficiency. PLoS One 2011;6(1):e16187. [PubMed: 21249153]
44. Schulze A Creatine deficiency syndromes. Handb Clin Neurol 2013;113:1837–1843. [PubMed: 23622406]
45. Stockler S, Holzbach U, Hanefeld F, Marquardt I, Helms G, Requart M, Hanicke W, Frahm J. Creatine deficiency in the brain: a new, treatable inborn error of metabolism. Pediatr Res 1994;36(3):409–413. [PubMed: 7808840]
46. Kan HE, Meeuwissen E, van Asten JJ, Veltien A, Isbrandt D, Heerschap A. Creatine uptake in brain and skeletal muscle of mice lacking guanidinoacetate methyltransferase assessed by magnetic resonance spectroscopy. J Appl Physiol 2007;102(6):2121–2127. [PubMed: 17347380]
47. Zaiss M, Bachert P. Exchange-dependent relaxation in the rotating frame for slow and intermediate exchange -- modeling off-resonant spin-lock and chemical exchange saturation transfer. NMR Biomed 2013;26(5):507–518. [PubMed: 23281186]
48. Xu J, Zaiss M, Zu Z, Li H, Xie J, Gochberg DF, Bachert P, Gore JC. On the origins of chemical exchange saturation transfer (CEST) contrast in tumors at 9.4 T. NMR Biomed 2014;27(4):406–416. [PubMed: 24474497]
49. Zaiss M, Xu J, Goerke S, Khan IS, Singer RJ, Gore JC, Gochberg DF, Bachert P. Inverse Zspectrum analysis for spillover-, MT-, and T1 -corrected steady-state pulsed CEST-MRI--application to pH-weighted MRI of acute stroke. NMR Biomed 2014;27(3):240–252. [PubMed: 24395553]
50. Ryoo D, Xu X, Li Y, Tang JA, Zhang J, van Zijl PCM, Liu G. Detection and Quantification of Hydrogen Peroxide in Aqueous Solutions Using Chemical Exchange Saturation Transfer. Anal Chem 2017;89(14):7758–7764. [PubMed: 28627877]
51. Lauzon CB, van Zijl P, Stivers JT. Using the water signal to detect invisible exchanging protons in the catalytic triad of a serine protease. J Biomol NMR 2011;50(4):299–314. [PubMed: 21809183]
52. Provencher SW. Estimation of metabolite concentrations from localized in vivo proton NMR spectra. Magn Reson Med 1993;30(6):672–679. [PubMed: 8139448]
53. Provencher SW. Automatic quantitation of localized in vivo 1H spectra with LCModel. NMR Biomed 2001;14(4):260–264. [PubMed: 11410943]
54. Renema WKJ, Schmidt A, van Asten JJ, Oerlemans F, Ullrich K, Wieringa B, Isbrandt D, Heerschap A. MR spectroscopy of muscle and brain in guanidinoacetate methyltransferase (GAMT)-deficient mice: validation of an animal model to study creatine deficiency. Magn Reson Med 2003;50(5):936–943. [PubMed: 14587004]
55. t Zandt Hi Groof Ad, Renema W, Oerlemans F, Klomp D, Wieringa B, Heerschap A,. Presence of (phospho) creatine in developing and adult skeletal muscle of mice without mitochondrial and

cytosolic muscle creatine kinase isoforms. The Journal of physiology 2003;548(3):847–858. [PubMed: 12640020]

Author Manuscript
Author Manuscript
Author Manuscript
Author Manuscript

Author Manuscript
Author Manuscript
Author Manuscript
Author Manuscript

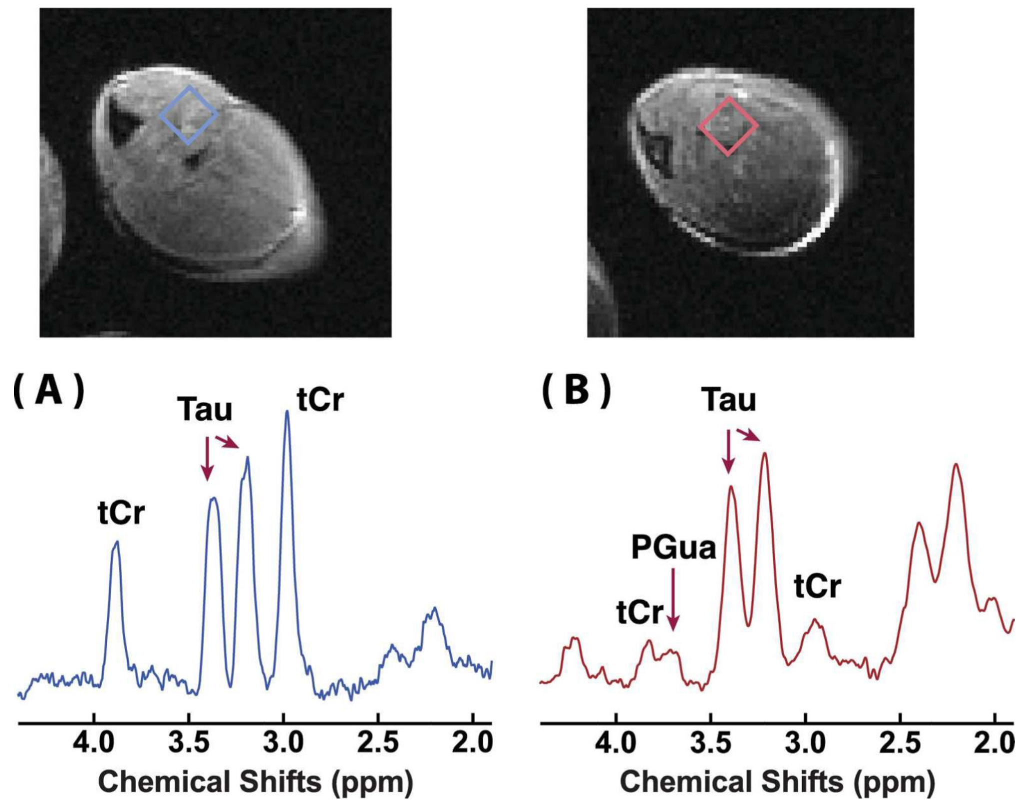

Figure 1.

In vivo ^{1}H NMR spectra of the skeletal muscle of (A) a WT mouse and (B) a GAMT−/− mouse. The corresponding T_2 weighted images (RARE sequence, in-plane resolution 170 × 170 μm^2, slice thickness 1.5 mm) are also shown. The rectangles indicated on the T_2 weighted images were selected as volumes of interest (VOIs) for the spectra. The assignment of the MRS peaks is also indicated.

Author Manuscript
Author Manuscript
Author Manuscript
Author Manuscript

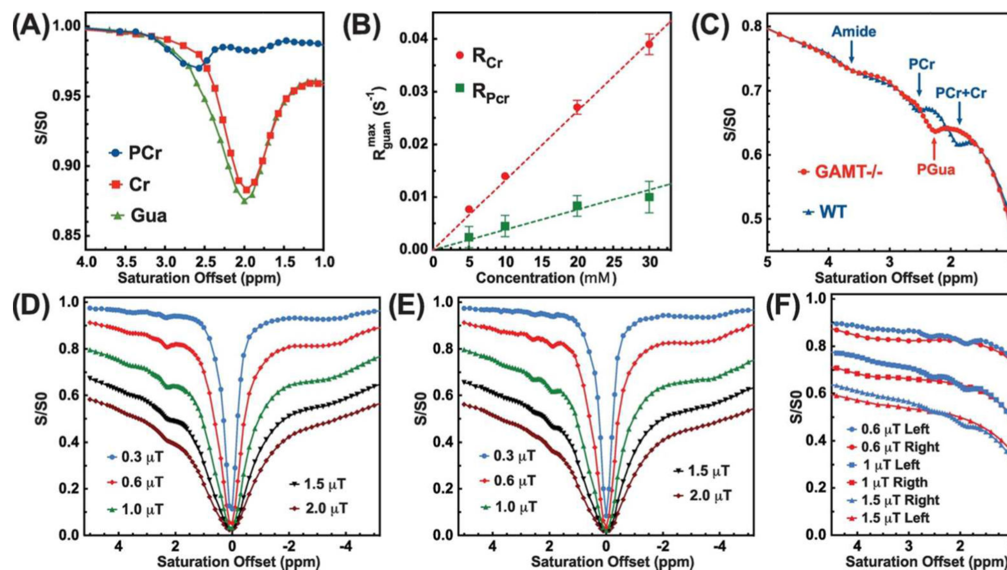

Figure 2.

(A) The Z-spectra of 30 mM PCr (blue), Cr (red) and Gua (green) solutions recorded using CW-CEST with 1 μT saturation power and 3 s length. (B) The concentration dependence of the Cr and PCr CEST signal R_{guan}^{max} at 2 and 2.5 ppm, respectively. The values were obtained from peak intensities of the Cr/PCr resonances in the Z-spectra and the measured R1 values (Eq. 1). The dashed lines (y = 1.3×10–3·x and y = 3.8×10–4·x) are drawn for visual guidance of the linearity of the concentration dependence. (C) The aligned averaged Z-spectra of GAMT −/− (n=3) and WT mice (n=3) collected with a saturation power of 1 μT (3 s length). The assignment of the CEST peaks is indicated. Typical full Z-spectra recorded on the calf muscle of the GAMT−/− mice (D) and the WT mice (E) using CW-CEST with the saturation powers and lengths of 0.3 μT (4 s), 0.6 μT (4 s), 1 μT (3 s), 1.5 μT (3 s), and 2 μT (2 s). (F) Comparisons of the left (1 to 5 ppm, blue lines) and right (−1 to −5 ppm, red lines) sides of Z-spectra recorded on the WT mice with saturation powers of 0.6 μT, 1 μT and 1.5 μT. The right sides of the Zspectra (−1 to −5 ppm) were flipped to the positive side of Z-spectra for clarity.

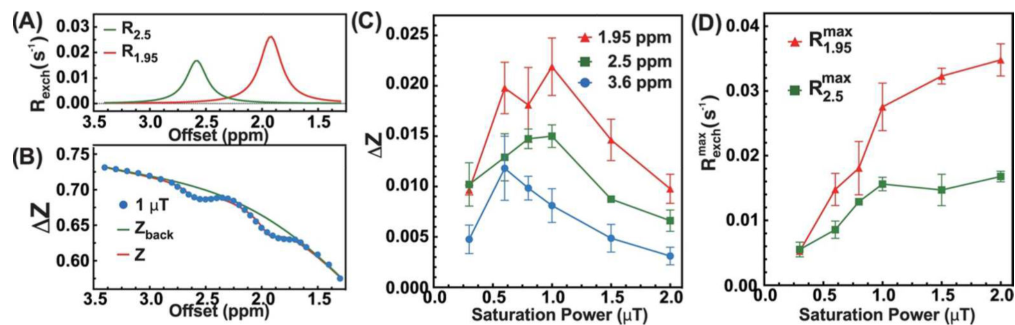

Figure 3.

(A) Typical $R_{2.5}$ and $R_{1.95}$ curves extracted using the two-peak PLOF method. (B) The corresponding fitting results (Z_{back} and Z) of one Z-spectrum collected on a WT mouse (R^2 =0.9974) with 1 μT saturation power. The frequency range between 1.3 and 3.4 ppm was utilized for the fitting and three sections, i.e. 1.3–1.7 ppm, 2.25–2.35 ppm and 2.83–3.4 ppm, were selected for the background fitting. (C) The observed CEST signals (Z) at 3.6 ppm, 2.5 ppm and 1.95 ppm as a function of saturation power. (D) The extracted $R_{2.5}^{max}$ and $R_{1.95}^{max}$ as a function of saturation power.

Author Manuscript
Author Manuscript
Author Manuscript
Author Manuscript

Author Manuscript
Author Manuscript
Author Manuscript
Author Manuscript

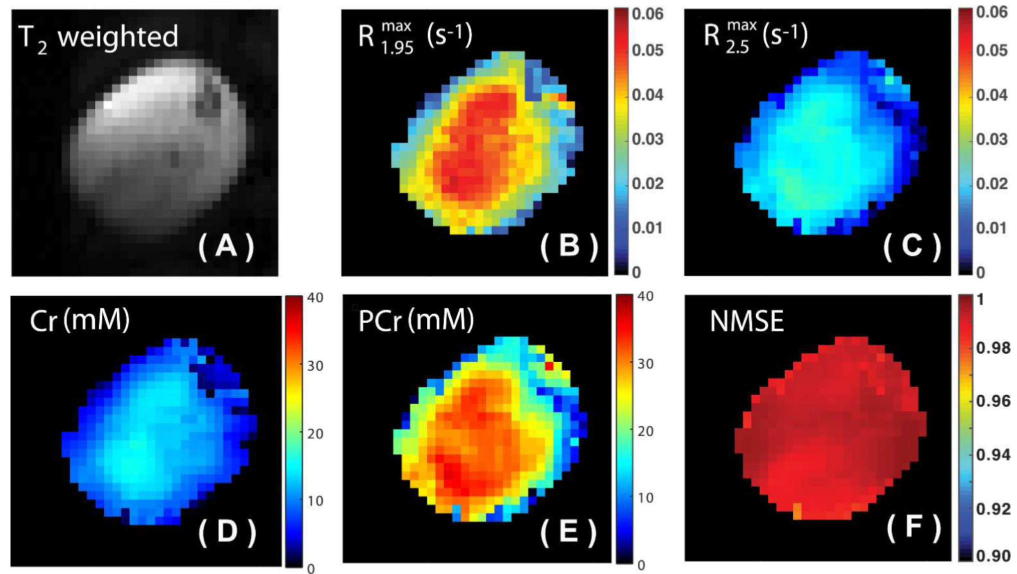

Figure 4.
(A) T_2 weighted image of the mouse hind leg used for anatomical guidance. The extracted maps of (B) $R_{1.95}^{max}$ and (C) $R_{2.5}^{max}$ determined by the PLOF method using the Z-spectrum recorded with a saturation power of 1 μT. (D) The Cr and (E) PCr concentration maps calculated using Eqs. 9 and 10, respectively. (F) The NMSE map calculated using Eq. 11 for evaluating the PLOF fitting.